ACES Asian Chemical Editorial Society

DOI: 10.1002/cnma.201700037

CHEMNANOMAT
Full Paper

Electrode Materials

SPECIAL ISSUE

Supramolecular Assembly of 1D Pristine Carbon Nanotubes and 2D Graphene Oxides into Macroscopic All-Carbon Hybrid Sponges for High-Energy-Density Supercapacitors

Kening Wan,[a] Siliang Liu,[a] Chao Zhang,*[a] Le Li,[a] Zhe Zhao,[a] Tianxi Liu,*[a] and Yi Xie[b]

Abstract: The rational design and targeted synthesis of macroscopic and ultralight all-carbon sponges with satisfying electron/proton conductivity through a simple and environmentally friendly approach is challenging. Herein, three-dimensional carbon nanotube-graphene oxide (CNT-GO) hybrid hydrogels have been constructed by the gelation of an aqueous dispersion of graphene oxide (GO) induced by pristine carbon nanotubes (CNTs) without any additives or other crosslinkers. Upon reduction of CNT-GO hydrogels and removal of water by freeze-drying, the resulting carbon nanotube-graphene (CNT-G) aerogels exhibit a unique all-carbon continuous framework with a hierarchical porosity that allows high-rate transport of electrolyte ions and electrons throughout the electrode matrix. As a result, they show high specific energy (31.3 $Wh\,kg^{-1}$), high specific capacitance with excellent rate performance (≈71% retention at 10 $A\,g^{-1}$) and cycling stability (≈100% retention at 10 $A\,g^{-1}$ for 5000 cycles) in two electrode systems, and thus great potential as promising electrode materials for next-generation supercapacitors.

Introduction

The increasing energy demands and the growth in portable electronic devices require the development of next-generation energy-storage systems. Supercapacitors, one of the promising alternative energy-storage systems, are able to satisfy these requirements due to their relatively fast charge and discharge rates, high energy densities, and long lifetimes.[1] Based on different energy-storage mechanisms, supercapacitors can be divided into two types: electrical double layer capacitors (EDLCs) and pseudocapacitors. Compared with pseudocapacitors, EDLCs, which store energy by means of the separation of surface charges, are regarded as the most easily commercialized supercapacitors and can achieve an extremely high cyclic stability and excellent rate capability. In order to overcome the few drawbacks such as relatively low specific energy, the development of new types of electrode materials with enhanced electrical conductivity and higher available surface area are required for boosting the energy-storage performance in both high power delivery rate and large specific energy.[2]

Graphene, a two-dimensional (2D) carbon material, is considered as a promising electrode material for EDLCs on account of its high surface area, excellent conductivity, large carrier mobility and high mechanical/chemical stability.[3] Furthermore, the assembly of 2D graphene into graphene aerogels (GAs) can achieve a highly continuous framework that allows the rapid access of electrolyte ions and the fast transport of electrons.[4] Although some novel methods, such as solution-processed vertical deposition,[6] and chemical vapor deposition,[7] have also been reported for the construction of GAs, the simple and easily processed sol–gel methods are considered as an easily scalable strategy to prepare GAs.[8] However, several drawbacks of the sol–gel methods for the formation of GAs have to be solved. First, the sol–gel methods for the preparation of GAs are typically starting from graphene oxide (GO), and excess reducing agents (like Vitamin C, hydrazine hydrate, sodium borohydride),[9] which may greatly influence the performance of GAs, are usually hard to remove and will inevitably reduce the electrical conductivity of the resultant GAs. Second, it is widely recognized that the mechanical strength of GAs typically depends on the intermolecular forces between stacked graphene sheets, so it is a great challenge to obtain high-strength GAs solely relying on graphene bricks.[10,11] Third, the sizes of the macropores of GAs are hard to precisely control without templates, except for the production of GAs using nickel foam, polymer spheres as templates. However, removing

[a] K. Wan, S. Liu, Dr. C. Zhang, L. Li, Z. Zhao, Prof. T. Liu
State Key Laboratory for Modification of Chemical Fibers and Polymer Materials
College of Materials Science and Engineering
Donghua University
Shanghai 201620 (P.R. China)
E-mail: czhang@dhu.edu.cn
txliu@dhu.edu.cn

[b] Prof. Y. Xie
Hefei National Laboratory for Physical Sciences at Microscale Collaborative Innovation Center of Chemistry for Energy Materials
University of Science & Technology of China
Hefei, Anhui 230026 (P.R. China)

Supporting information for this article can be found under: http://dx.doi.org/10.1002/cnma.201700037.

This manuscript is part of a Special Issue on 2D Materials for Energy Applications. A link to the Table of Contents will appear here once the Special Issue is assembled.

these templates often leads to severe problems, such as high cost, low yield and unavoidable residue of templates after etching. To summarize, the construction of 3D GAs using a newly explored template-free method is attractive and challenging.[12]

To date, the hybridization of 2D graphene with one-dimensional (1D) carbon nanotubes (CNTs) is considered as an efficient method to improve the performances of graphene-based electrodes. As reported, the CNT-graphene (CNT-G) hybrids are promising electrode materials for supercapacitors,[7e,13] and the CNT-G hybrids possessing a bi-continuous conductive network can significantly enhance the energy-storage performance.[7a,14] These strategies illustrate unique synergistic effects of CNTs and graphene, where 1D CNTs can bridge 2D graphene to construct 3D all-carbon nanostructures with improved electrical conductivity. Moreover, the enlarged accessible surface area due to the introduction of unique porosity within the hybrids greatly boosts the transport rates of electrolyte ions into the internal parts of the electrode matrix, where a large specific capacitance with high rate capacitance can be further benefited.

Herein, we report a simple and environmentally friendly approach to prepare CNT-G hybrid sponges via a supramolecular assembly between CNTs and GO, followed by a subsequent hydrothermal treatment. By utilizing pristine CNTs as a unique crosslinker, the gelation of aqueous suspension of GO forms due to non-covalent bonds (e.g., π–π stacking interactions, van der Waals force) between CNTs and GO, which enable 1D CNTs to crosslink 2D GO sheets into 3D CNT-GO hybrid hydrogels. A subsequent hydrothermal reduction method is utilized to reduce GO within the CNT-GO hydrogels, thus to form the CNT-G hydrogels. After removing the water by freeze drying, the macroscopic and ultralight CNT-G hybrid sponges are successfully obtained, which exhibit outstanding electrochemical capacitive performance for supercapacitors with high specific capacitances, excellent rate capabilities and long cycle life.

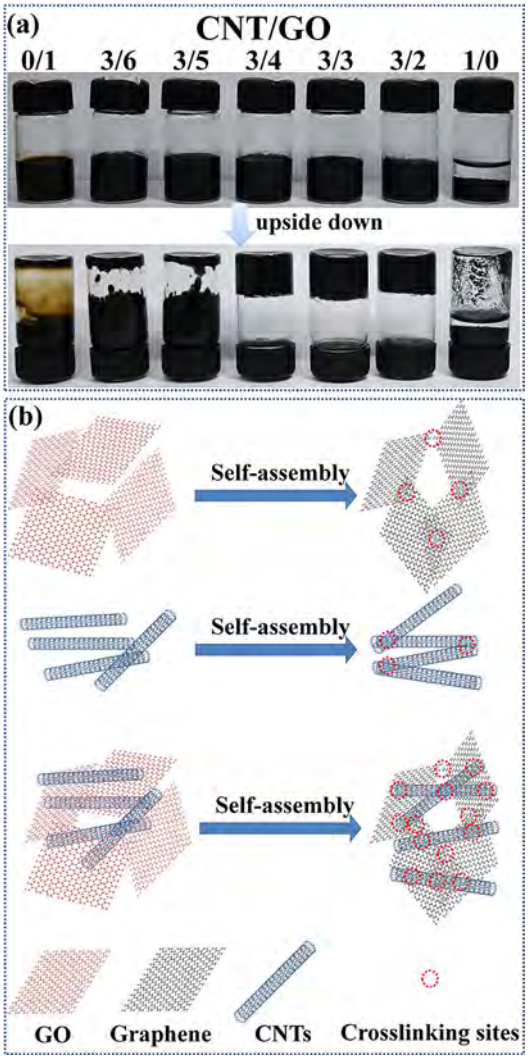

Figure 1. (a) Photographs of the aqueous suspensions of GO mixed with pristine CNTs with the CNT/GO mass ratios of 0/1, 3/6, 3/5, 3/4, 3/3, 3/2 and 1/0, from left to right. (b) Schematic of 3D network formation by the non-covalent bonds between graphene and CNTs.

Results and Discussion

The fabrication process for the construction of CNT-GO hybrid hydrogels is extremely simple involving a sonication to promote a uniform dispersion of pristine CNTs into an aqueous suspension of GO (the single-layer structure of GO is evidenced by the transmission electron microscopy (TEM) image in Figure S1 in the Supporting Information). An immediate gelation forms when the mixture of CNT powder and GO suspension is simply sonicated. As shown in Figure 1 a, in order to indicate the crosslinking effects of pristine CNTs on the CNT-GO hydrogels and optimize the composition of the resultant hybrid aerogels, different initial mass ratios of CNT/GO are utilized to prepare the CNT-GO hybrid hydrogels, which are named as CNT3GO6 (CNT/GO: 3/6), CNT3GO5 (CNT/GO: 3/5), CNT3GO4 (CNT/GO: 3/4), CNT3GO3 (CNT/GO: 3/3) and CNT3GO2 (CNT/GO: 3/2), while the concentration of the aqueous suspension of GO is kept at 8 mg mL^{-1}. The CNT-GO hydrogels only form in the CNT3GO4, CNT3GO3 and CNT3GO2 samples. We propose a mechanism to explain the gelation of GO suspension in the presence of CNTs, as exhibited in Figure 1 b. Gelation does not occur for the aqueous suspension of neat GO or CNTs, indicating that few crosslinking sites form in their respective suspensions. When mixing the aqueous suspension of GO and pristine CNTs with a proper mass ratio, a percolation threshold for the formation of 3D continuous framework might occur, namely, a gelation could take place after homogeneously mixing GO and pristine CNTs in suspension assisted with sonication. Actually, pristine CNTs can be homogeneously dispersed in the aqueous suspension of GO and the mixture can stay stable for a long time. Figure S2 exhibits the digital pictures captured for the diluted aqueous dispersion of CNTs, GO and CNT3GO3 after being left standing for two weeks. The pristine CNTs cannot form a uniform aqueous suspension after a long sonication. The suspension of GO (2 mg mL^{-1}) is extremely stable. When the CNT3GO3 hydrogel was diluted with water until the suspension contains 2 mg mL^{-1} of GO. The suspension is black and rather stable, indicating that the GO has the ability to uniformly disperse pristine CNTs in aqueous

media. The TEM images of the CNT3GO3 samples were characterized to confirm the formation of crosslinking sites between GO and CNTs. The individual GO sheet prefers to interact with the surrounded CNTs in suspension, resulting in the formation of the CNT-GO hybrid with a configuration of 2D GO bridged with 1D CNTs (Figure S3). For comparison, the TEM images of neat GO (Figure S1) and CNTs (Figure S4) indicate few crosslinking sites in these neat component samples. Although the hydrogels could be directly constructed by the gelation of aqueous dispersions of GO induced by pristine CNTs and the mechanically stable CNT-GO hybrid aerogels can be prepared by a simple freezing drying (Figure S5), hydrothermal reduction method was used to further reduce GO into graphene inside these hybrid hydrogels for the following two reasons. First, the simple and green hydrothermal reduction method has been used here to reduce the GO inside the CNT-GO hybrid hydrogels in order to improve the electrical conductivity which is vital for the use as electrode materials for supercapacitors. Second, the hydrothermal reduction of the CNT-GO hybrid aerogels into the CNT-G hybrid aerogels promotes mechanical strength and thermal stability through further crosslinking of graphene sheets within the CNT-G hybrid aerogels. The successful reduction of GO in the resultant sponges after the hydrothermal treatment has been illustrated by measuring the FTIR spectra of the CNT3G3 sample before and after the hydrothermal treatment, as shown in Figure S6. The peaks associated with the oxygen-containing groups such as the C-*O*-C ($\approx$1400 cm^{-1}), C—OH ($\approx$1100 cm^{-1}) and C=O ($\approx$1650 cm^{-1}) bands can be clearly observed in the spectrum of CNT/GO (3/3) aerogel sample. The intensities of these oxygen-containing groups strongly decrease after the hydrothermal reduction, illustrating the elimination of these groups in the CNT3G3 aerogel sample. Meanwhile, the persistence of C=O stretching bands implies that the C=O groups are difficult to remove by hydrothermal treatment. It should be noted that, although a gelation does not occur for the aqueous suspension of neat GO, a subsequent hydrothermal treatment for neat GO suspension also produces GAs after a subsequent freeze-drying process.

The morphology and porous nanostructure of the resulting CNT-G sponges are revealed by scanning electron microscopy (SEM) observations. As shown in Figure 2, all the aerogels exhibit highly porous nanostructures. The 1D CNTs with diameters of 20–30 nm (evidenced by Figure S4) are attached randomly to the graphene frameworks without obvious aggregation, thus forming a 3D network structure with both macropores and mesopores. In addition, GAs and CNTs themselves possess micropores due to closely stacked porosity. Particularly, with different mass ratios of CNT/GO, these aerogels, although they exhibit similar 3D networks, present different porous characteristics. With higher loadings of CNTs, plenty of larger macropores with thinner solid walls are produced. This is because with increased loadings of CNTs (from GAs to CNT3G2 sample), more crosslinking sites form due to non-covalent bonds between CNTs and graphene sheets, leading to more stable 3D frameworks with fewer graphene sheets stacked up.

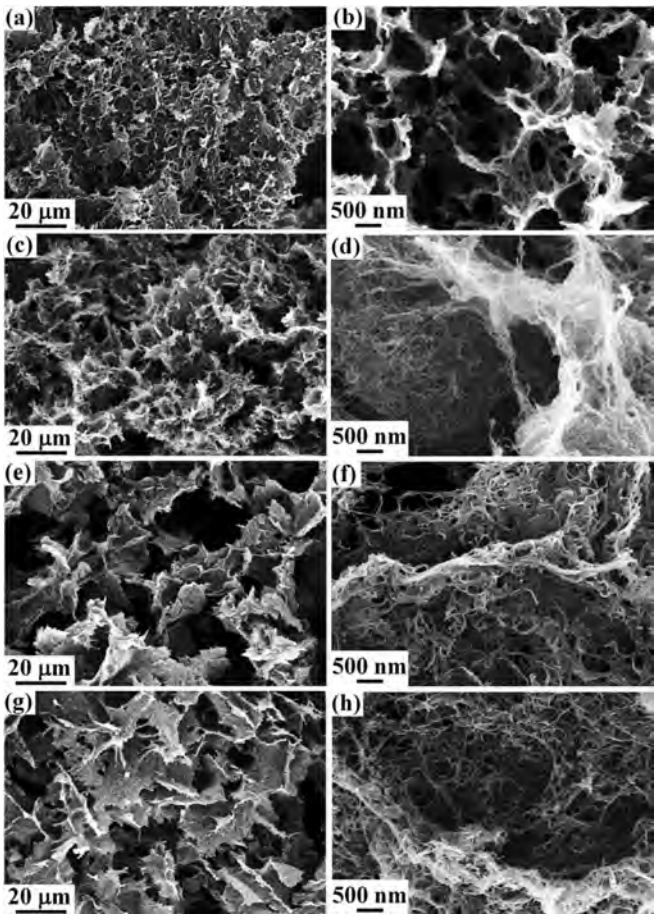

Figure 2. Cross-section SEM images of (a, b) GAs, (c, d) CNT3G4, (e, f) CNT3G3 and (g, h) CNT3G2 at low and high magnifications, respectively.

Elemental analysis based on the combustion method was performed in order to illustrate the composition of the CNT-G hybrid sponges. The elemental analysis results (see Table 1) indicate that all the hybrid sponges contain more than 85 wt% of carbon. The C/O weight ratios of GAs, CNT3G4, CNT3G3, CNT3G2 and CNTs can be calculated to be 5.3, 11.3, 13.7, 17.1 and 109, respectively. The existence of oxygen in GAs and CNT-G hybrids aerogels confirms the residual oxygen-containing groups within the graphene sheets, which might provide addition pseudocapacitive performance, boosting the final electrochemical energy-storage performances.

Table 1. Composition and nitrogen sorption data of CNT-G aerogels, GAs and CNTs at various initial mass ratios of CNT/GO.

Samples	Elemental analysis [wt%]			S_{BET} [m^2 g^{-1}]	Pore volume [mL g^{-1}]		
	C	H	O		Total	Micro	Meso
GAs	76.6	1.4	14.5	288	0.26	0.08	0.18
CNT3G4	85.6	1.0	7.6	259	0.81	0.04	0.77
CNT3G3	89.3	0.8	6.5	232	0.80	0.03	0.77
CNT3G2	92.1	0.5	5.4	173	0.54	0.02	0.52
CNTs	98.1	0.2	0.9	151	0.69	0.01	0.68

Moreover, in order to verify the resulting CNT-G sponges have high Brunauer–Emmett–Teller (BET) surface area, large pore volume and wide pore size distribution, nitrogen sorption investigations have been taken, as shown in Figure 3, Figure S7

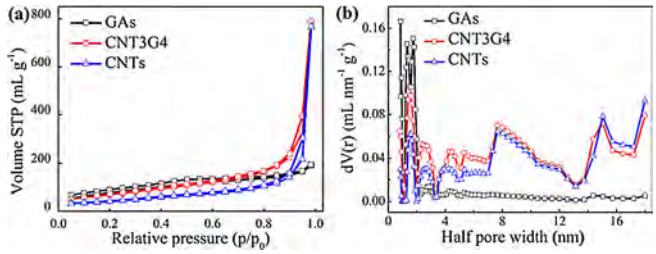

Figure 3. Nitrogen adsorption–desorption isotherms and pore size distributions of CNT3G4, GAs and CNTs.

and summarized in Table 1. The nitrogen adsorption–desorption isotherm curves indicate that the CNT-G sponges possess many more macropores and mesopores than neat GAs. The CNTs exhibit a lower surface area than GAs and CNT-G samples, indicating that the combination of CNTs with graphene contributes to higher surface area. Though the surface areas of the CNT-G sponges are slightly lower than that of GAs, the largely increased pore volumes (especially mesopore volumes) of the CNT-G sponges indicate that the presence of CNTs within the CNT-G sponges inhibits the re-stacking of graphene and introduces additional porosities.

The unique 3D conductive frameworks and hierarchical porosities make these CNT-G sponges ideal candidates for various applications in energy-based fields. We attempt to apply them as electrode materials for supercapacitors and evaluate their electrochemical capacitive properties. First of all, the electrochemical capacitive performance was tested in a 6 mol L^{-1} KOH electrolyte in a three-electrode configuration. Cyclic voltammetry (CV) curves at scan rates ranging from 10 to 200 mV s^{-1} for various samples have been tested and are shown in Figure 4a. The CV curves present typical rectangular shapes without cathodic or anodic peaks, indicating that these electrodes exhibit the electrochemical double layer capacitive mechanism, which is consistent with the characteristics of other carbon-based electrodes.[15] Taking the CNT3G4 electrode as an example, the CV curves at the scan rate of 200 mV s^{-1} still remain a symmetrical rectangular shape with a slight deviation (Figure 4b), illustrating a fast charge and discharge capability. This excellent rate capacitance is also shown by galvanostatic charge/discharge curves (Figure S8a and S8b). The specific capacitance of the CNT3G4 electrode can reach 300 F g^{-1} at a current density of 2 A g^{-1}, which is much higher than those of CNTs (75 F g^{-1}) and GAs (153 F g^{-1}) at the same current density. What is more, the CNT-G sponges exhibit outstanding rate capacitances. With the increase of the current densities, their specific capacitances decrease very slowly. Particularly, the specific capacitance of the CNT3G4 electrode still remains 80% at a high current density of 20 A g^{-1} compared with that at 2 A g^{-1}. The large surface areas and appropriate pore size distributions are expected to provide effective channels for high-rate transport of ions and electrons throughout the electrode matrix.[16]

Electrochemical impedance spectroscopy (EIS) measurements are utilized to monitor the electrochemical process of the interfacial behaviors between electrodes and electrolytic ions. The Nyquist plots of the electrodes obtained by EIS measurements are displayed in Figure 4d. Nearly straight lines of all

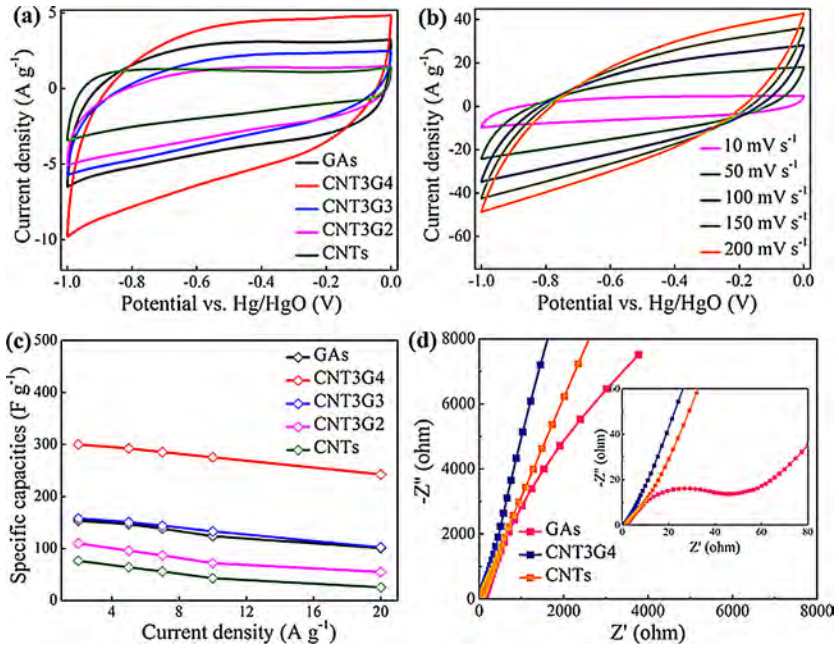

Figure 4. Electrochemical properties of CNT-G electrodes measured in a three-electrode configuration: (a) CV curves for GAs, CNT3G4, CNT3G3, CNT3G2 and CNTs at a scan rate of 10 mV s^{-1}. (b) CV curves for the CNT3G4 electrode at different scan rates. (c) The rate capacitances of all samples ranging from 2 to 20 A g^{-1}. (d) Nyquist plots of GAs, CNT3G4 and CNTs at the frequency range from 0.01 Hz to 10^6 Hz (inset is the enlargement of the high-frequency region).

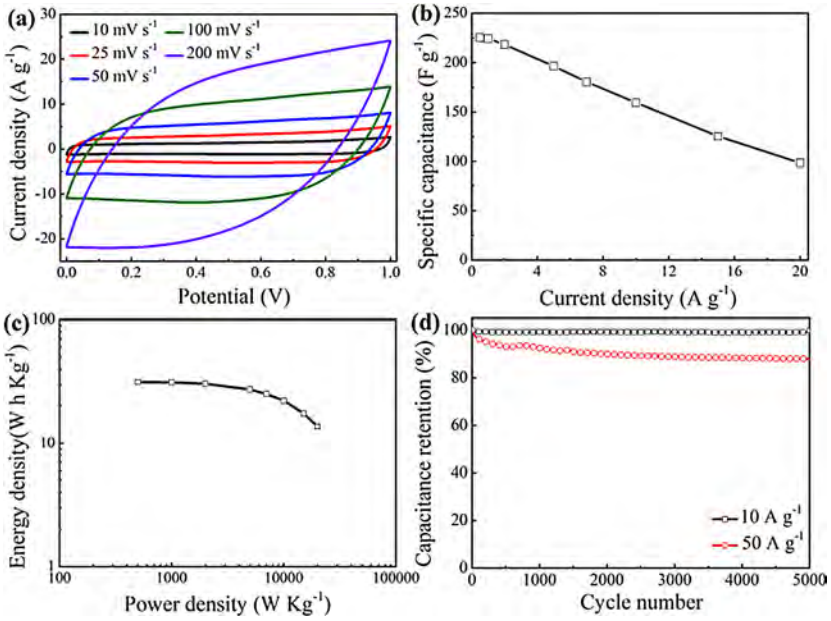

Figure 5. Electrochemical properties of the CNT3G4 electrodes assembled in a symmetric two-electrode supercapacitor: (a) CV curves for the CNT3G4 electrode at different scan rates. (b) The rate capacitances of the CNT3G4 electrode ranging from 0.5 to 20 A g^{-1}. (c) Ragone plots of the CNT3G4 electrode assembled in a supercapacitor. (d) Cycling stability of the CNT3G4 electrode at charge/discharge current densities of 10 and 50 A g^{-1}.

the electrodes in low frequency regions represent the ion diffusion and transport following an electrochemical double layer capacitive behavior. There are no obvious semicircles for the CNTs and CNT3G4 electrodes in high-frequency regions, indicating extremely fast ion diffusions of CNTs and CNT3G4 electrodes. The equivalent series resistance (ESR) for the CNT3G4 electrode (0.9 Ω), determined by taking the high frequency intercept on the *x* axis, is slightly lower than those of the CNTs (1.5 Ω) and GAs (2.4 Ω), revealing a fast movement of electrons within the CNT3G4 electrode.

To further evaluate the performance of the CNT3G4 electrode, a supercapacitor device using a two-electrode configuration was assembled and tested. As shown in Figure 5a, similar with the CV curves of the CNT3G4 electrode tested in a three-electrode system, the CV curves of the CNT3G4 electrode in a two-electrode configuration show regular rectangular shapes even at a high scan rate of 200 mV s^{-1}, indicating fast electron/ion diffusion channels within the CNT3G4 electrode. The relationships of specific capacitances as a function of current densities for the CNT3G4 electrode are calculated and presented in Figure 5b. The CNT3G4 electrode exhibits the highest specific capacitance of ≈225 F g^{-1} at 0.5 A g^{-1}. The capacitance retains as much as 71% of its initial value at 0.5 A g^{-1} as the current density increases to 10 A g^{-1}, indicating an excellent rate retention of capacitance. We also plot the Ragone figure, shown as Figure 5c, where the corresponding energy and power density are calculated from the galvanostatic charge/discharge curves. The as-assembled devices with the symmetric two-electrode configuration of both CNT3G4 electrodes deliver high energy density of 31.3 Wh kg^{-1} at a power density of 500 W kg^{-1}, and still retain 13.7 Wh kg^{-1} at a higher power density of 20 kW kg^{-1}. Cycling stability is an important factor for evaluating the performance of an electrode material. Cyclic stability for the resultant two-electrode supercapacitor devices was conducted using repeated galvanostatic charge/discharge cycles at 10 and 50 A g^{-1}, respectively (Figure 5d). In a 6 M KOH electrolyte, the supercapacitors using symmetric CNT3G4 electrodes keep almost 100% of the initial value after 5000 charge/discharge cycles at a current density of 10 A g^{-1}. Even at an extremely high current density up to 50 A g^{-1}, a capacitance retention larger than 88% can be achieved, indicating these hybrid aerogels show excellent cyclic stability for next-generation supercapacitors. The introduction of 1D CNTs as a unique nanospacer into the graphene matrix not only reduces the re-stacking of graphene but also contributes to building a unique 3D conductive framework providing a large accessible surface area with more efficient and shortened ion-diffusion pathways. Stable maintenance of the electrode microstructure derived from the strong interfacial interaction between graphene and CNTs might be another potential factor for the enhanced cycling stability, which is evidenced by the measurement of almost coincident EIS curves before and after cycling for the CNT3G4 electrode (Figure S9). Therefore, as mentioned above, the synergistic effects and optimized nanostructures cooperatively facilitate the resultant CNT-G hybrid aerogel's high specific capacitance, good rate capability and excellent long-term cycling stability.

Conclusions

The all-carbon CNT-G sponges can be simply obtained from the starting materials of pristine CNTs and GO. A solution-processed supramolecular assembly of CNTs and GO produces 3D nanostructured CNT-GO hydrogels, and then a reduction and freeze-drying process is utilized for the formation of CNT-G hybrid sponges. The resultant CNT-G sponges with a tailored

composition exhibit a large BET surface area (259 $m^2 g^{-1}$), a hierarchical pore size distribution, and suitable pore volume (0.81 $mL g^{-1}$). The CNT3G4 electrodes show superior electrochemical capacitive performances including the superior high energy densities (31.3 $Wh kg^{-1}$) and excellent rate capability (71% at from 1 to 10 $A g^{-1}$). The unique nanoscale structures, including 3D conductive frameworks, large active surface areas and excellent electrochemical properties, make these all-carbon CNT-G sponges ideal electrode materials for supercapacitors.

Experimental Section

Materials: Natural graphite powder (≈325 mesh) was purchased from Alfa Aesar. Deionized water was used throughout all the experiments. MWNTs (length: 10–30 μm, outer diameter: 20–30 nm, purity: 95%), produced by CVD method, were supplied by Chengdu Institute of Organic Chemistry, Chinese Academy of Sciences, China. All the other reagents were purchased from Sinopharm Chemical Reagent Co. Ltd. and used as received.

Preparation and purification of graphite oxide: Graphite oxide was synthesized by a modified Hummers' method. Typically, a mixture of graphite (5 g) and $NaNO_3$ (5 g) was placed in 230 mL of concentrated H_2SO_4. $KMnO_4$ (15 g) was added gradually with stirring and cooling, so that the temperature of the mixture was not allowed to reach 20 °C. The mixture was then maintained at 35 ± 3 °C for 30 min. After that, deionized water (460 mL) was slowly added to the mixture and the temperature was increased to 98 °C. After 15 min, the mixture was further treated with 350 mL deionized water and 25 mL 5% H_2O_2 solution, and then filtered, washed successively with 5% diluted HCl solution completely until sulfate could not be detected with $BaCl_2$. The resulting solid filtration residue was suspended in water under ultrasonication for half an hour, followed by centrifugation at 4000 rpm for 10 min. The resulting supernatant was dried via evaporation of water under vacuum. Finally, the solid was dispersed again in water (8.0 $mg mL^{-1}$) by ultrasonication for 2 h and centrifuging at 10000 rpm for 20 min to further remove any aggregates.

Fabrication of CNT-GO hydrogels and CNT-G aerogels: Designed amounts of pristine CNTs were added into the as-obtained GO aqueous suspensions. The mixture was ultrasonicated for 30 min in order to uniformly disperse CNTs into the GO suspension. The CNT-GO hybrid hydrogels can be formed when the initial mass ratios of CNT/GO are higher than 3/5. The as-obtained CNT-GO hydrogels were hydrothermally treated at 180 °C for 12 h, thus to obtain the CNT-G hydrogels. Afterwards, the water was removed from the hydrogel samples by freeze-drying for 48 h. The CNT-G hybrid aerogels with different mass ratios of CNT/GO can be obtained and named as GAs (from neat GO), CNT3G4 (from CNT/GO:3/4), CNT3G3 (from CNT/GO:3/3) and CNT3G2 (from CNT/GO:3/2).

Characterization: The morphology of the samples was evaluated by field-emission scanning electron microscopy (FESEM, Ultra 55) and transmission electron microscopy (TEM, Tecnai G2 20 TWIN). Fourier transform infrared (FTIR) spectra of CNT/GO sample before and after hydrothermal reduction were taken by a Nicolet Nexus-670 (Nicolet, US) in the range of 500–4000 cm^{-1}. The elemental analyses were performed by Elementar Vario EL III (Elementar Analysensysteme GmbH, Germany) based on JY/T 017-1996 general rules for elemental analyzer. Nitrogen sorption tests were measured at −196 °C in a N_2 atmosphere after degassing the samples at 100 °C under vacuum for 24 hours using a Quantachrome Autosorb-iQ-AG porosimeter. The apparent surface area was calculated by applying the Brunauer–Emmett–Teller (BET) model to the isotherm data points of the adsorption branch in the relative pressure range $p/p_0 < 0.3$. The pore size distribution was calculated from nitrogen sorption data using the nonlocal density functional theory (NLDFT) equilibrium model method for slit pores provided by Quantachrome data reduction software ASiQWin Version 4.01.

Electrochemical characterization: The electrochemical capacitive behaviors were measured with CHI 660D electrochemical workstation. In a standard three-electrode setup, the working electrodes were prepared by mixing 80 wt% active materials, 10 wt% carbon black (Super P), and 10 wt% polyvinylidene fluoride (PVDF) in *N*-methyl-2-pyrrolidone (NMP), followed by drying it on a graphite paper current collector (1 × 1 cm^2) in vacuum at 80 °C overnight. The typical loading density for the resultant electrode is approximately 1.0 $mg cm^{-2}$. A platinum wire and Hg/HgO electrode was used as the counter electrode and the reference electrode, respectively, and a 6.0 M KOH aqueous solution was used as the electrolyte. Cyclic voltammetry (CV) was performed within a potential range of −1–0 V vs. Hg/HgO at scan rates of 10–200 $mV s^{-1}$. Galvanostatic charge/discharge testing was done from −1.0 to 0 V vs. Hg/HgO electrode at current densities of 2, 5, 7, 10 and 20 $A g^{-1}$. Electrochemical impedance spectroscopy (EIS) was performed in the frequency range from 0.01 to 10^6 Hz at open circuit potential with an AC voltage amplitude of 5 mV. In a standard two-electrode setup, the working electrodes with the same active material loadings were prepared using a similar fabrication method as for the three-electrode setup, and a 6.0 M KOH aqueous solution was used as the electrolyte. Cyclic voltammetry (CV) was performed within a potential range of 0–1 V at scan rates of 10–200 $mV s^{-1}$. Galvanostatic charge/discharge testing was done from 0 to 1 V at a current density of 0.5, 1, 2, 5, 7, 10 and 20 $A g^{-1}$.

Acknowledgements

We are grateful for the financial support from the National Natural Science Foundation of China (Grants No. 21504012, 51125011 and 51433001), the Fundamental Research Funds for the Central Universities (No. 16D110617), the Program of Shanghai Academic Research Leader (No. 17XD1400100) and the Natural Science Foundation of Shanghai (No. 17ZR1439900).

Keywords: carbon nanotubes · graphene · hierarchical porosity · supercapacitors · supramolecular assembly

[1] a) M. F. El-Kady, R. B. Kaner, *Nat. Commun.* **2013**, *4*, 1475; b) J. Bae, M. K. Song, Y. J. Park, J. M. Kim, M. Liu, Z. L. Wang, *Angew. Chem. Int. Ed.* **2011**, *50*, 1683–1687; *Angew. Chem.* **2011**, *123*, 1721–1725; c) G. Wei, S. Neelam, S. Li, L. Zheng, A. L. M. Reddy, C. Lijie, V. Robert, Z. Qing, W. Bingqing, P. M. Ajayan, *Nat. Nanotechnol.* **2011**, *6*, 496–500; d) J. Chmiola, C. Largeot, P. L. Taberna, P. Simon, Y. Gogotsi, *Science* **2010**, *328*, 480–483.

[2] a) X. Yang, C. Cheng, Y. Wang, L. Qiu, D. Li, *Science* **2013**, *341*, 534–537; b) Y. Gogotsi, P. Simon, *Science* **2011**, *334*, 917–918.

[3] a) A. K. Geim, *Science* **2009**, *324*, 1530–1534; b) K. S. Novoselov, V. I. Fal'Ko, L. Colombo, P. R. Gellert, M. G. Schwab, K. Kim, *Nature* **2012**, *490*, 192–200; c) M. F. El-Kady, S. Veronica, D. Sergey, R. B. Kaner, *Science* **2012**, *335*, 1326–1330.

[4] a) X. Wang, C. Lu, H. Peng, X. Zhang, Z. Wang, G. Wang, *J. Power Sources* **2016**, *324*, 188–198; b) T. T. Chen, W. L. Song, L. Z. Fan, *Electrochim. Acta* **2015**, *165*, 92–97; c) Y. Ma, Y. Chen, *Natl. Sci. Rev.* **2015**, *2*, 40–53.

[5] a) W. Lv, Y. Tao, W. Ni, Z. Zhou, F. Y. Su, X. C. Chen, F. M. Jin, Q. H. Yang, *J. Mater. Chem.* **2011**, *21*, 12352 – 12357; b) H. D. Pham, V. H. Pham, T. V. Cuong, T. D. Nguyenphan, J. S. Chung, E. W. Shin, S. Kim, *Chem. Commun.* **2011**, *47*, 9672 – 9674; c) P. Chen, J. J. Yang, S. S. Li, Z. Wang, T. Y. Xiao, Y. H. Qian, S. H. Yu, *Nano Energy* **2013**, *2*, 249 – 256; d) Y. X. Xu, K. X. Sheng, C. Li, G. Q. Shi, *ACS Nano* **2010**, *4*, 4324 – 4330; e) Z. H. Tang, S. L. Shen, J. Zhuang, X. Wang, *Angew. Chem. Int. Ed.* **2010**, *49*, 4603 – 4607; *Angew. Chem.* **2010**, *122*, 4707 – 4711; f) L. Chen, B. Wei, X. Zhang, C. Li, *Small* **2013**, *9*, 2331 – 2340; g) H. Huang, P. Chen, X. Zhang, Y. Lu, W. Zhan, *Small* **2013**, *9*, 1397 – 1404; h) Z. Sui, Q. Meng, X. Zhang, R. Ma, B. Cao, *J. Mater. Chem.* **2012**, *22*, 8767 – 8771; i) Z. Sui, X. Zhang, Y. Lei, Y. Luo, *Carbon* **2011**, *49*, 4314 – 4321; j) X. Zhang, Z. Sui, B. Xu, S. Yue, Y. Luo, W. Zhan, B. Liu, *J. Mater. Chem.* **2011**, *21*, 6494 – 6497.

[6] a) Y. Zhang, X. Cao, Z. Li, D. Zhao, *Appl. Phys. A* **2016**, *122*, 1 – 7; b) J.-J. Shao, S.-D. Wu, S.-B. Zhang, W. Lv, F.-Y. Su, Q.-H. Yang, *Chem. Commun.* **2011**, *47*, 5771 – 5773.

[7] a) Z. Fan, J. Yan, L. Zhi, Q. Zhang, T. Wei, J. Feng, M. Zhang, W. Qian, F. Wei, *Adv. Mater.* **2010**, *22*, 3723 – 3728; b) X. Dong, Y. Ma, G. Zhu, Y. Huang, J. Wang, M. B. Chanpark, L. Wang, W. Huang, P. Chen, *J. Mater. Chem.* **2012**, *22*, 17044 – 17048; c) X. Cao, Y. Shi, W. Shi, G. Lu, X. Huang, Q. Yan, Q. Zhang, H. Zhang, *Small* **2011**, *7*, 3163 – 3168; d) J. S. Lee, H. J. Ahn, J. C. Yoon, J. H. Jang, *Phys. Chem. Chem. Phys.* **2012**, *14*, 7938 – 7943; e) Q. Cheng, J. Tang, J. Ma, H. Zhang, N. Shinya, L. C. Qin, *Phys. Chem. Chem. Phys.* **2011**, *13*, 17615 – 17624.

[8] a) H. Bai, C. Li, X. Wang, G. Shi, *Chem. Commun.* **2010**, *46*, 2376 – 2378; b) H. Bai, K. Sheng, P. Zhang, C. Li, G. Shi, *J. Mater. Chem.* **2011**, *21*, 18653 – 18658; c) C. Huang, H. Bai, C. Li, G. Shi, *Chem. Commun.* **2011**, *47*, 4962 – 4964; d) Y. Xu, Q. Wu, Y. Sun, H. Bai, G. Shi, *ACS Nano* **2010**, *4*, 7358 – 7362.

[9] S. Pei, H. M. Cheng, *Carbon* **2012**, *50*, 3210 – 3228.

[10] Z. Han, Z. Tang, P. Li, G. Yang, Q. Zheng, J. Yang, *Nanoscale* **2013**, *5*, 5462 – 5467.

[11] H. Hu, Z. Zhao, W. Wan, Y. Gogotsi, J. Qiu, *Adv. Mater.* **2013**, *25*, 2219 – 2223.

[12] a) Y. E. Shin, Y. J. Sa, S. Park, J. Lee, K. H. Shin, S. H. Joo, H. Ko, *Nanoscale* **2014**, *6*, 9734 – 9741; b) W. L. Li, K. Lu, J. Y. Walz, *Int. Mater. Rev.* **2012**, *57*, 37 – 60.

[13] D. Yu, L. Dai, *J. Phys. Chem. Lett.* **2010**, *1*, 467 – 470.

[14] S. Y. Yang, K. H. Chang, H. W. Tien, Y. F. Lee, S. M. Li, Y. S. Wang, J. Y. Wang, C. C. M. Ma, C. C. Hu, *J. Mater. Chem.* **2011**, *21*, 2374 – 2380.

[15] a) G. P. Hao, W. C. Li, D. Qian, A. H. Lu, *Adv. Mater.* **2010**, *22*, 853 – 857; b) Y. Tao, M. Endo, K. Kaneko, *J. Am. Chem. Soc.* **2009**, *131*, 904 – 905.

[16] a) Z. Li, B. Li, Z. Liu, D. Li, H. Wang, Q. Li, *Electrochim. Acta* **2016**, *190*, 378 – 387; b) C. Zhu, T. Liu, F. Qian, T. Y. Han, E. B. Duoss, J. D. Kuntz, C. M. Spadaccini, M. A. Worsley, Y. Li, *Nano Lett.* **2016**, *16*, 3448 – 3456; c) H. Xie, S. Tang, D. Li, S. Vongehr, X. Meng, *ChemSusChem* **2016**, DOI: 10.1002/cssc.201600150.

Manuscript received: February 13, 2017
Revised: March 7, 2017
Accepted Article published: March 12, 2017
Final Article published: ■■ ▮▮, 0000

FULL PAPER

Electrode Materials

Kening Wan, Siliang Liu, Chao Zhang, Le Li, Zhe Zhao, Tianxi Liu,* Yi Xie*

■■ – ■■

Supramolecular Assembly of 1D Pristine Carbon Nanotubes and 2D Graphene Oxides into Macroscopic All-Carbon Hybrid Sponges for High-Energy-Density Supercapacitors

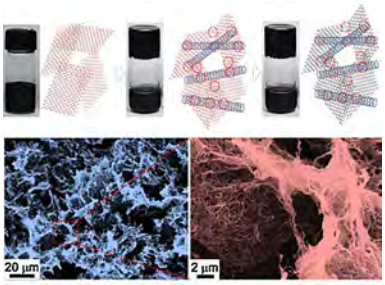

All-carbon hybrid aerogels consisting of pristine carbon nanotubes (CNTs) and graphene oxide (GO) have been prepared using an extremely simple approach. The potential use of such three-dimensional all-carbon aerogels with net-like porous carbon walls as a promising electrode material for supercapacitors has also been demonstrated.